tvst

Article

The Mlc1 Promoter Directs Müller Cell-specific Gene Expression in the Retina

Yosuke Danjo[1,2,*], Youichi Shinozaki[1,2,*], Akiyo Natsubori[3], Yuto Kubota[1,2], Kenji Kashiwagi[4], Kenji F. Tanaka[5], and Schuichi Koizumi[1,2]

[1] Department of Neuropharmacology, Interdisciplinary Graduate School of Medicine, University of Yamanashi, Yamanashi, Japan
[2] GLIA Center, University of Yamanashi, Yamanashi, Japan
[3] Sleep Disorders Project, Tokyo Metropolitan Institute of Medical Science, Tokyo, Japan
[4] Department of Ophthalmology, Interdisciplinary Graduate School of Medicine, University of Yamanashi, Yamanashi, Japan
[5] Department of Neuropsychiatry, Keio University School of Medicine, Tokyo, Japan

Correspondence: Schuichi Koizumi, Department of Neuropharmacology, Interdisciplinary Graduate School of Medicine, University of Yamanashi, 1110 Shimokato, Chuo, Yamanashi 409-3898, Japan.
e-mail: skoizumi@yamanashi.ac.jp

Received: June 17, 2021
Accepted: November 27, 2021
Published: January 18, 2022

Keywords: astrocytes; gene expression; Mlc1; Müller cells; retina

Citation: Danjo Y, Shinozaki Y, Natsubori A, Kubota Y, Kashiwagi K, Tanaka KF, Koizumi S. The Mlc1 promoter directs Müller cell-specific gene expression in the retina. Transl Vis Sci Technol. 2022;11(1):25, https://doi.org/10.1167/tvst.11.1.25

Purpose: Because the importance of glia in regulating brain functions has been demonstrated, genetic technologies that manipulate glial cell-specific gene expression in the brain have become essential and have made great progress. However, it is unknown whether the same strategy that is used in the brain can be applied to the retina because retinal glia differs from glia in the brain. Here, we aimed to find a method for selective gene expression in Müller cells (characteristic glial cells in the retina) and identified Mlc1 as a specific promoter of Müller cells.

Methods: Mlc1-*tTA*::Yellow-Cameleon-Nano$^{tetO/tetO}$ (YC-Nano) mice were used as a reporter line. YC-Nano, a fluorescent protein, was ectopically expressed in the cell type controlled by the Mlc1 promotor. Immunofluorescence staining was used to identify the cell type expressing YC-Nano protein.

Results: YC-Nano-positive ($^+$) signals were observed as vertical stalks in the sliced retina and spanned from the nerve fiber layer through the outer nuclear layer. The density of YC-Nano$^+$ cells was higher around the optic nerve head and lower in the peripheral retina. The YC-Nano$^+$ signals colocalized with vimentin, a marker of Müller cells, but not with the cell markers for blood vessels, microglia, neurons, or astrocytes.

Conclusions: The Mlc1 promoter allows us to manipulate gene expression in Müller cells without affecting astrocytes in the retina.

Translational Relevance: Gene manipulation under control of Mlc1 promoter offers novel technique to investigate the role of Müller cells.

Introduction

Glial cells, non-neuronal cells, are the major cell component in the central nervous system. They contain three major cell types: microglia, oligodendrocytes, and astrocytes. Astrocytes play an essential role in neuronal information processing and connectivity.[1,2] They provide metabolic support for neurons and contribute to the regulation of blood flow and energy homeostasis.[3,4] Astrocytes control synaptic connections by producing synaptogenic molecules and exerting phagocytic functions.[5,6] They also release various neurotrophic factors, such as brain-derived neurotrophic factor,[4,7,8] ciliary neurotrophic factor,[9,10] and insulin-like growth factor,[11–13] thereby contributing to neuronal survival, the formation of neural circuits, and regeneration after injury. Under pathological conditions, astrocytes become reactive and express neuroprotective or neurodegenerative phenotypes.[4,14]

In the retina, astrocyte-lineage cells are composed of two types of cells: astrocytes and Müller cells (retina-specific cells). Retinal astrocytes exist in the nerve fiber layer (NFL) in which they elongate their processes and form honeycomb patterns in the inner surface of the retina. Their endfeet tightly attach to and

Copyright 2022 The Authors

This work is licensed under a Creative Commons Attribution-NonCommercial-NoDerivatives 4.0 International License.

cover the blood vessels and the axon bundles derived from the retinal ganglion cells.[15] Müller cells are characterized by a vertical stalk that spans through the retina. Their cell bodies reside in the inner nuclear layer (INL), and their processes ensheath the synapses and blood vessels in the inner and outer plexiform layers (IPL and OPL). Müller cells also play essential roles in retinal functions, such as modulating neurotransmission,[3,16,17] supporting neurite outgrowth,[18–20] and maintaining ion homeostasis.[4,21] Under pathological conditions, Müller cells become reactive[22] and undergo reprogramming to acquire stem cell-like functions that enable the regeneration of retinal neurons; this occurs in fish but not mammals.[23]

To distinguish the two astrocyte-lineage cells, cell type-specific markers are used. For example, retinal astrocytes under normal conditions are enriched in glial fibrillary acidic protein (GFAP),[24] whereas Müller cells strongly express vimentin,[25,26] glutamine synthase,[27] and glutamate/aspartate transporter (GLAST) proteins.[28] To control the gene expression of specific cell types, the promoter that is highly active in the cell type is used. However, retinal astrocytes and Müller cells share many enriched genes,[29] and thus brain astrocyte-specific gene manipulation is not always applied to retinal astrocytes. For example, gene manipulation under the GLAST promoter is astrocyte-selective in the brain, whereas it is Müller cell-selective in the retina.[30] We have previously developed a flexible accelerated STOP-tetO-knockin (FAST) system to efficiently manipulate gene expression in vivo[31]; the promoter of megalencephalic leukoencephalopathy with the subcortical cysts 1 (*Mlc1*) gene was used to achieve astrocyte-specific gene manipulation.[32] Although this system enabled us to monitor astrocytic activity[33] and astrocyte-specific overexpression[34] or knockdown of target genes,[35] it is unknown whether retinal astrocytes or Müller cells are affected by the promoter. Here, we demonstrate that the Mlc1 promoter can selectively control gene expression of Müller cells without affecting astrocytes in the retina.

Methods

All reagents and antibodies used in the present study are listed in the Table.

Animals

All animals used in this study were obtained, housed, cared for, and used in accordance with the "Guiding Principles in the Care and Use of Animals in the Field of Physiological Sciences" published by the Physiological Society of Japan and with the previous approval of the Animal Care Committee of Yamanashi University (Chuo, Yamanashi, Japan). Our experimental conditions adhered to the ARVO Statement for the Use of Animals in Ophthalmic and Vision Research. Mice were maintained in a pathogen-free and temperature- and humidity-controlled facility (23°C and 55%, respectively) with a 12 hour (6:00 AM to 6:00 PM) light-dark cycle. The mice in each cage had free access to food and water. For visualization, we crossed Mlc1-*tTA* mice with YC-Nano$^{tetO/tetO}$ mice (Mlc1-*tTA*::YC-Nano$^{tetO/tetO}$), as previously reported.[33] We used nine young adult (3 months old) male mice in the present study. We found no significant infertility or reproductive abnormalities in this transgenic mouse. To obtain Mlc1-*tTA*::YC-Nano$^{tetO/tetO}$ mouse, we prepared two or three breeding cages (one male with 2–3 females per cross). For analysis of fluorescence signals in the normal conditions, we used three retinae from different mice. In the experiment for intravitreal *N*-methyl-D-aspartate (NMDA) injection, six retinae from six mice were used for saline- and NMDA-treated groups, respectively.

Preparation of Flat-Mount Retinae and Retinal Slices

Mice were anesthetized with a mixture of medetomidine (0.9 mg/kg body weight [BW]), midazolam (12.0 mg/kg BW), and butorphanol (15.0 mg/kg BW). Eyes were enucleated and immersed in 4% of paraformaldehyde for 30 minutes at room temperature and then dissected, as previously reported.[36] The isolated retinae were post-fixed overnight at 4°C. One retina from the mouse was then cut into a quadrant. The other retina was cut in half and it was further cut into half to obtain quadrant retinae. The other half of the retina was used to prepare retinal sections (20–30 sections from one retina). Each quadrant retina was used as one flat-mount retinal sample for immunohistochemistry. Immunostained retinae were mounted with Slow Fade Gold antifade reagent (Thermo Fisher Scientific, Waltham, MA, USA). For retinal slices, the enucleated eyes were fixed in 4% of paraformaldehyde for 1 day at 4°C and soaked in 20% sucrose/phosphate-buffered saline (PBS) for 2 day. The samples were then embedded in Tissue-Tek optimal cutting temperature compound (Sakura Fintek, Tokyo, Japan) and frozen. All specimens were cut into 20 µm thick slices and attached to a glass slide.

Table. Materials Used in the Present Study

Reagent Type (Species) or Resource	Designation	Source or Reference	Identifiers	Additional Information
Strain, strain background (Mus musculus)	Mlc1-tTA::YC-Nano$^{tetO/tetO}$ mice	Kanemaru et al. 2014	NA	
Antibodies	Anti-Brn3a (Goat polyclonal)	Santacruz	RRID: AB_2167511 Santacruz: sc-31984	(1:300)
Antibodies	Anti-Iba1(Rabbit polyclonal)	Fuji Film-Wako	RRID:AB_839504 FUJI-Wako: 019-19741	(1:500)
Antibodies	Anti-GFAP (Rat monoclonal)	Invitrogen	RRID: AB_2532994 Invitrogen: 13-0300	(1:500)
Antibodies	Anti-Vimentin (Chick polyclonal)	Abcam	RRID: AB_77824 Abcam: ab24525	(1:1000)
Antibodies	Anti-S100β (Mouse monoclonal)	Sigma-Aldrich	RRID: AB_477499 Sigma: s2532	(1:500)
Antibodies	Anti-GLAST (Rabbit polyclonal)	Abcam	RRID: AB_955879 Abcam: ab41751	(1:100)
Antibodies	Isolectin B4, biotinylated	VECTOR Laboratories	RRID: AB_2314661 VECTOR: B-1205	(1:25)
Antibodies	Streptavidin-Alexa555	Thermo Fisher Scientific	RRID: AB_2307336 Thermo: S21381	(1:1000)
Antibodies	Paraformaldehyde (PFA)	Fuji film-Wako	162-16065	4%(wt/vol)
Chemicals, peptides, and recombinant proteins	Bovine serum albumin (BSA)	Sigma-Aldrich	A2153	
Chemicals, peptides, and recombinant proteins	Butorphanol	Meiji Seika Pharma Co., Ltd.	N/A	
Chemicals, peptides, and recombinant proteins	Triton X-100	Sigma-Aldrich	T7878	
Chemicals, peptides, and recombinant proteins	4′,6-diamidino-2-phenylindole, dihydrochloride (DAPI)	DOJINDO	D523	(1:1000)
Chemicals, peptides, and recombinant proteins	Medetomidine hydrochloride	Laboratorios Syva	N/A	
Chemicals, peptides, and recombinant proteins	Midazolam	Maruishi Pharmaceutical. Co., Ltd.	N/A	
Chemicals, peptides, and recombinant proteins	*N*-methyl-D-aspartate	Sigma-Aldrich	M2362	
Chemicals, peptides, and recombinant proteins	Slow Fade Gold Antifade Mountant	Thermo Fisher Scientific	S36936	
Chemicals, peptides, and recombinant proteins	Tissue-Tek O.C.T. compound	Sakura finetek	4583	
Software, algorithm	Image J/FIJI	https://imagej.net/Fiji	RRID: SCR_003070	
Others	Cryostat	Leica Biosystems	Leica C1520	
Others	FV-1200	Olympus	N/A	

N/A, not applicable.

Immunohistochemistry

For the flat-mount retinae, the samples were permeabilized and blocked with 5% normal goat serum in 2% Triton X-100-containing PBS (PBST) for 1 hour at room temperature. For the retinal slices, tissues were permeabilized and blocked with 5% goat serum in 0.3% PBST. Then samples were incubated with primary antibodies at 4°C for 3 days (for flat-mount) and overnight (for slices). The flat-mount retinae and retinal slices were washed 3 times with PBST at room temperature for 10 minutes and incubated with secondary antibodies for 1 hour at room temperature. Fluorescent images were acquired with a laser scanning confocal microscope (FV1200; Olympus, Tokyo, Japan).

Intravitreal NMDA Injection

To investigate Mlc1 promoter activity under pathological conditions, we intravitreally injected NMDA to the YC-Nano mice, as previously reported.[37] Six male Mlc1-*tTA*::YC-Nano$^{tetO/tetO}$ mice were anesthetized with intraperitoneal injection of a mixture of medetomidine hydrochloride (0.3 mg/kg), midazolam (4 mg/kg), and butorphanol tartrate (5 mg/kg), followed by instillation of 0.5% bupivacaine (5 µL/eye). Then, a small incision was made with a 30-gauge needle 0.5 to 1.0 mm behind the limbus in the superior region of the globe of the eye. NMDA (2 µL at 10 mM in saline) was injected into the right eyes using a glass syringe with a 30-gauge needle. For control, the sham operation was performed by injecting a vehicle (2 µL of saline) into the left eyes, and the absence of retinal ganglion cell (RGC) degeneration was confirmed. To estimate the NMDA-caused damages of RGCs, we quantified the changes in the number of Rbpms$^+$ RGCs in the ganglion cell layer (GCL) of the flat-mounted retina.

Antibodies and Dyes

The following primary antibodies were used in the present study: rabbit anti-Iba1 (1:500, Wako, 019-19741), rat anti-GFAP (1:500, Invitrogen, 13-0300), rabbit anti-GLAST (1:200, Abcam, ab41751), mouse anti-S100β (1:500, Sigma, s2532), chick anti-vimentin (1:1000, Abcam, ab24525), and goat anti-Brn3a (1:300, Santa Cruz, sc-31984). Nuclei were stained with 4′,6-diamidino-2-phenylindole (DAPI, 100 µg/mL, DOJINDO). Biotinylated isolectin B4 was purchased from Vector Laboratories (Burlingame, CA, USA). YC-Nano signals were highly stable and we did not use antibodies to visualize them. All Alexa-conjugated secondary antibodies and streptavidin were obtained from Thermo Fisher Scientific.

Data Analysis

To quantify colocalization of immunofluorescence images, we used Coloc 2 plugin of FUJI software (https://imagej.net/Fiji). Two fluorescence images were opened via FUJI and activated Coloc 2 by *Analyze-Colocalization-Coloc 2*. Statistical analysis was performed using Origin Pro2021 (Origin Lab, Northampton, MA, USA). Data were shown as mean ± SEM and comparison of multiple groups was performed by 1-way ANOVA followed by Fisher's least significant difference (LSD) test.

Results

Mlc1-*tTA*::YC-Nano$^{tetO/tetO}$ mice (YC-Nano mice) were used to visualize Mlc1 promoter-mediated gene expression. In these mice, YC-Nano-positive (YC-Nano$^+$) fluorescence signals were observed throughout the flat-mount retinae (Fig. 1A). In the GCL and nerve fiber layers (NFLs), punctate YC-Nano$^+$ signals were observed in the center (see Fig. 1A-a, approximately 500 µm from the optic nerve head) and mid-peripheral retina (see Figs. 1A-b, 1A-c). In the peripheral retina, the number of YC-Nano$^+$ signals was smaller (see Fig. 1A-d). We then investigated the detailed spatial patterns of YC-Nano$^+$ signals in the different layers of the neural retina (see Fig. 1B). In the NFL, the YC-Nano$^+$ signals showed amorphous patterns of 10 to 20 µm (see Fig. 1B-a). They attached to adjacent DAPI$^+$ signals and included some vesicle-like structures that, however, never contained DAPI. In the GCL, the YC-Nano$^+$ signals showed small punctate structures surrounding DAPI$^+$ signals (see Fig. 1B-b). In the IPL, relatively close to the GCL, the signals were punctate with fine process-like structures (see Fig. 1B-c). In the IPL close to the INL, most of the YC-Nano$^+$ signals were similar to those in Figure 1B-c, but some of them showed tubular structures (see Fig. 1B-d, arrows). In the retinal slices, we analyzed three areas that were adjacent to the (1) optic nerve head (see Fig. 1C-a), (2) mid-peripheral retina (see Fig. 1C-b), and (3) peripheral retina (see Fig. 1C-c). The density of YC-Nano$^+$ cells was the highest in the mid-peripheral retina and the lowest in the peripheral retina. YC-Nano$^+$ cells were observed as vertical stalks that spanned the retina (see Fig. 1D). In the NFL and GCL, they exhibited thick endfeet-like structures surrounding the DAPI$^+$ signals (see Fig. 1D-a). In the

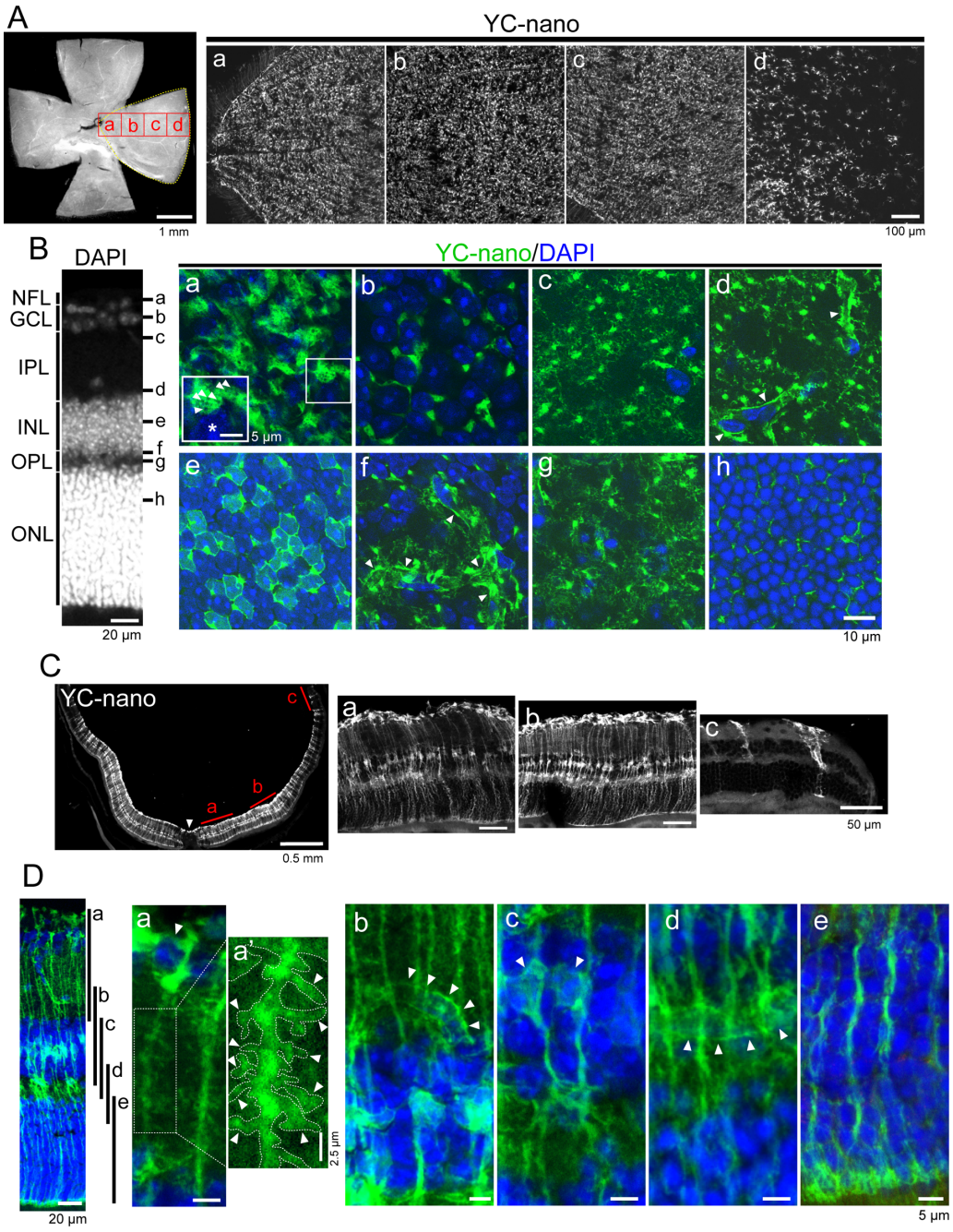

Figure 1. **Spatial patterns of fluorescence signals in Mlc1-*tTA*::YC-Nano$^{tetO/tetO}$ mice.** (**A**) The spatial distribution of YC-Nano^{+} signals in the GCL and NFL of flat-mount retina. Images were taken sequentially from near the optic nerve head to the peripheral retina (**Aa–Ad**). At the limbus of the retina, the density of YC-Nano^{+} cells was small (**Ad**). (**B**) The more detailed spatial arrangement of YC-Nano^{+} signals in each neuronal layer of the retina. (**Ba**) In the NFL, the YC-Nano^{+} signals were irregular with some vacuole-like structures (*arrows*). They surrounded DAPI signals (*asterisk*). (**Bb**) In the GCL, YC-Nano^{+} signals filled the gap between the DAPI signals. (**Bc**) In the IPL, YC-Nano^{+} signals showed a circular spatial pattern with fine protrusions. (**Bd**) Near the INL, some YC-Nano^{+} signals showed a tubular spatial arrangement (*arrows*). (**Be**) In the INL, the YC-Nano^{+} signals were pentagonal or hexagonal, and DAPI was encapsulated within it. (**Bf**) In the boundary region between the INL and the OPL, some YC-Nano^{+} signals were tubular (*arrows*). (**Bg**) In the OPL, YC-Nano^{+} signals were circular with fine processes. (**Bh**) In the ONL, the YC-Nano^{+} signal was fibrous between the DAPI signals. (**C**) The spatial arrangement of YC-Nano^{+} cells in a retinal slice. Magnified images were obtained from the area near the optic nerve head (**Ca**), from the mid-peripheral retina (**Cb**), and from the limbus of the retina (**Cc**). (**D**) Magnified images of the retinal slice. (**Da**) In the GCL, YC-Nano^{+} signals surrounded DAPI^{+} signals (*arrow*). (**Da'**) In the IPL, many fine process-like structures were observed (*arrows*). Tubular patterns were observed in IPL (**Db**) and OPL (**Dd**). (**Dc**) In the INL, some DAPI^{+} signals were incorporated in the YC-Nano^{+} signals. (**De**) The YC-Nano^{+} signals passed between DAPI. NFL, nerve fiber layer; GCL, ganglion cell layer; IPL, inner plexiform layer; INL, inner nuclear layer; OPL, outer plexiform layer; ONL, outer nuclear layer.

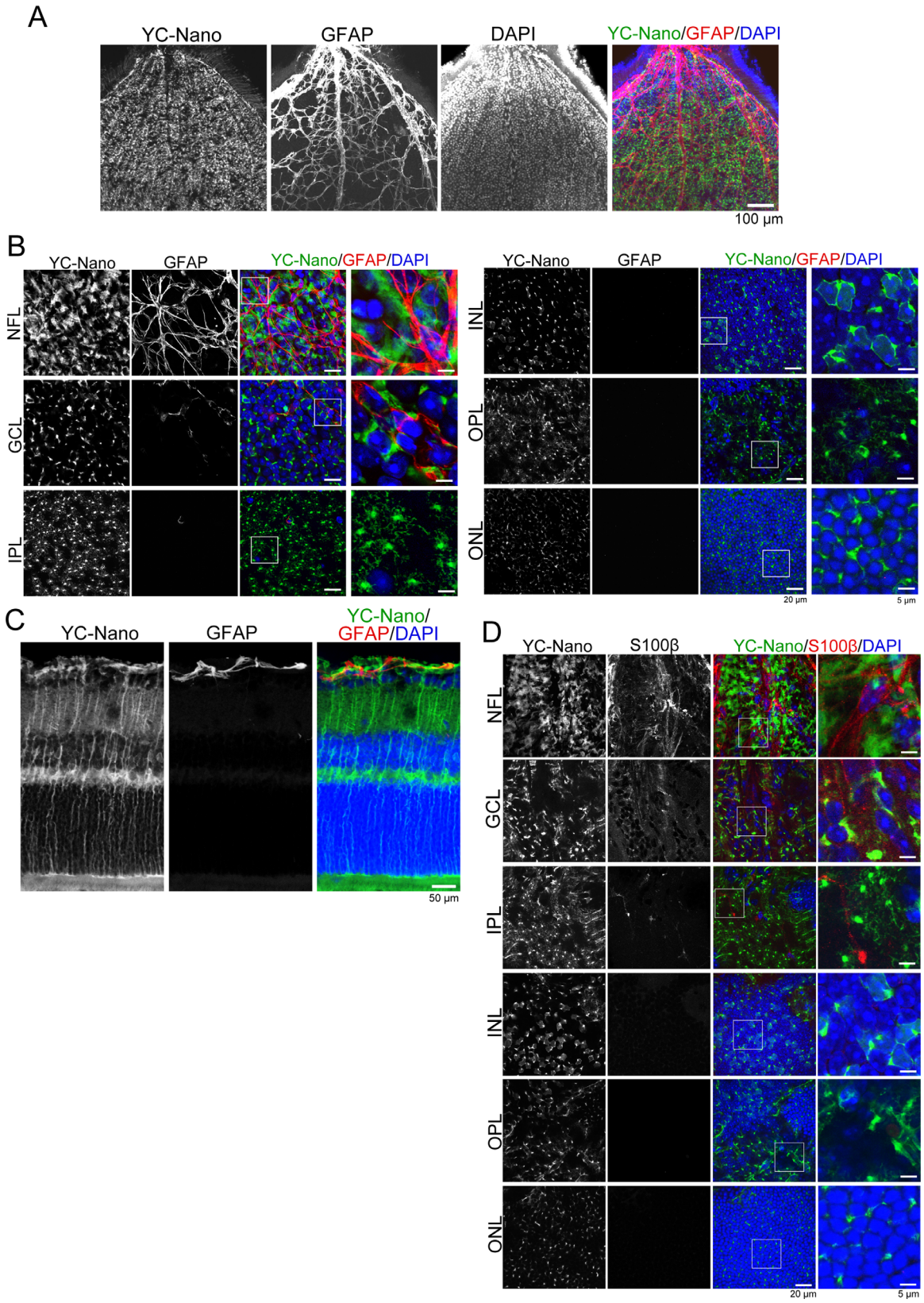

Figure 2. **YC-Nano is not expressed in retinal astrocytes.** (**A**) Low-magnification images of a flat-mount retina. GFAP^{+} signals showed honeycomb-like patterns. (**B**) Magnified images of each neural layer from **A**. The right panels are the enlarged images of the framed areas. (**C**) In the retinal slices, the GFAP^{+} signals were limited to the NFL and did not co-localize with the YC-Nano^{+} signals. (**D**) The S100ß signal distribution in the flat-mount retinae. The fiber-like S100ß$^{+}$ signal in the GCL/NFL did not colocalize with the YC-Nano^{+} signals.

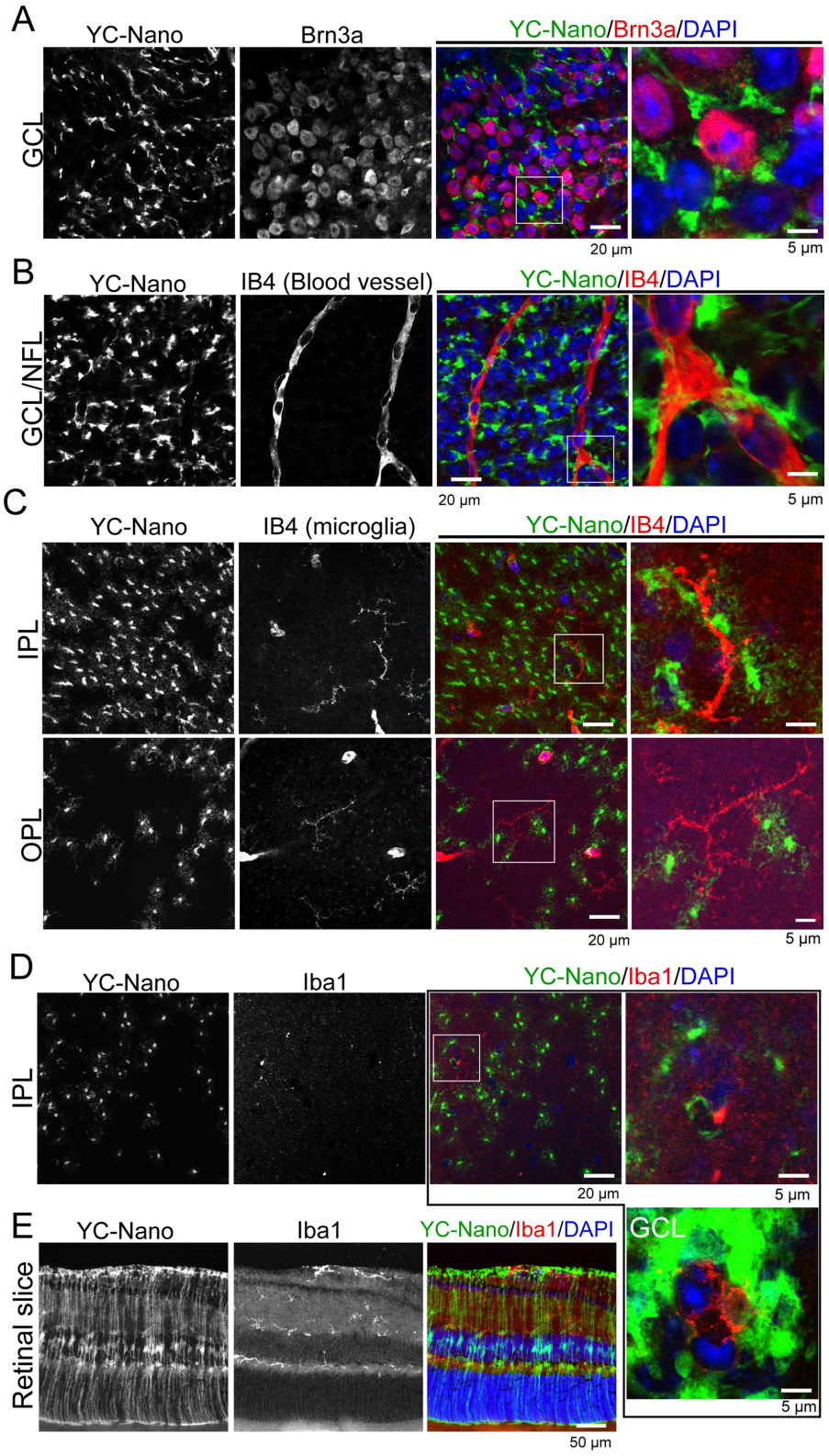

Figure 3. **YC-Nano is not expressed in retinal ganglion cells, blood vessels, or microglia.** (**A**) Brn3a$^+$ retinal ganglion cells do not express YC-Nano. The endfeet-like YC-Nano$^+$ signals surround the retinal ganglion cell body. (**B**) IB4$^+$ blood vessels in the ganglion cell layer (GCL) and nerve fiber layer (NFL) do not colocalize with YC-Nano$^+$ signals. The YC-Nano$^+$ cells attached their endfeet-like structures to the blood vessels. (**C–E**) IB4$^+$ or Iba1$^+$ microglia do not express YC-Nano. **C** IB4$^+$ microglia in the inner plexiform layer (IPL) or outer plexiform layer (OPL) showed no overlap with YC-Nano$^+$ signals but showed close apposition to each other and the microglial processes attached to the fine processes of YC-Nano$^+$ cells. Iba1$^+$ microglia also do not co-localize with YC-Nano$^+$ signals in either **D** flat-mount or **E** sliced retinae.

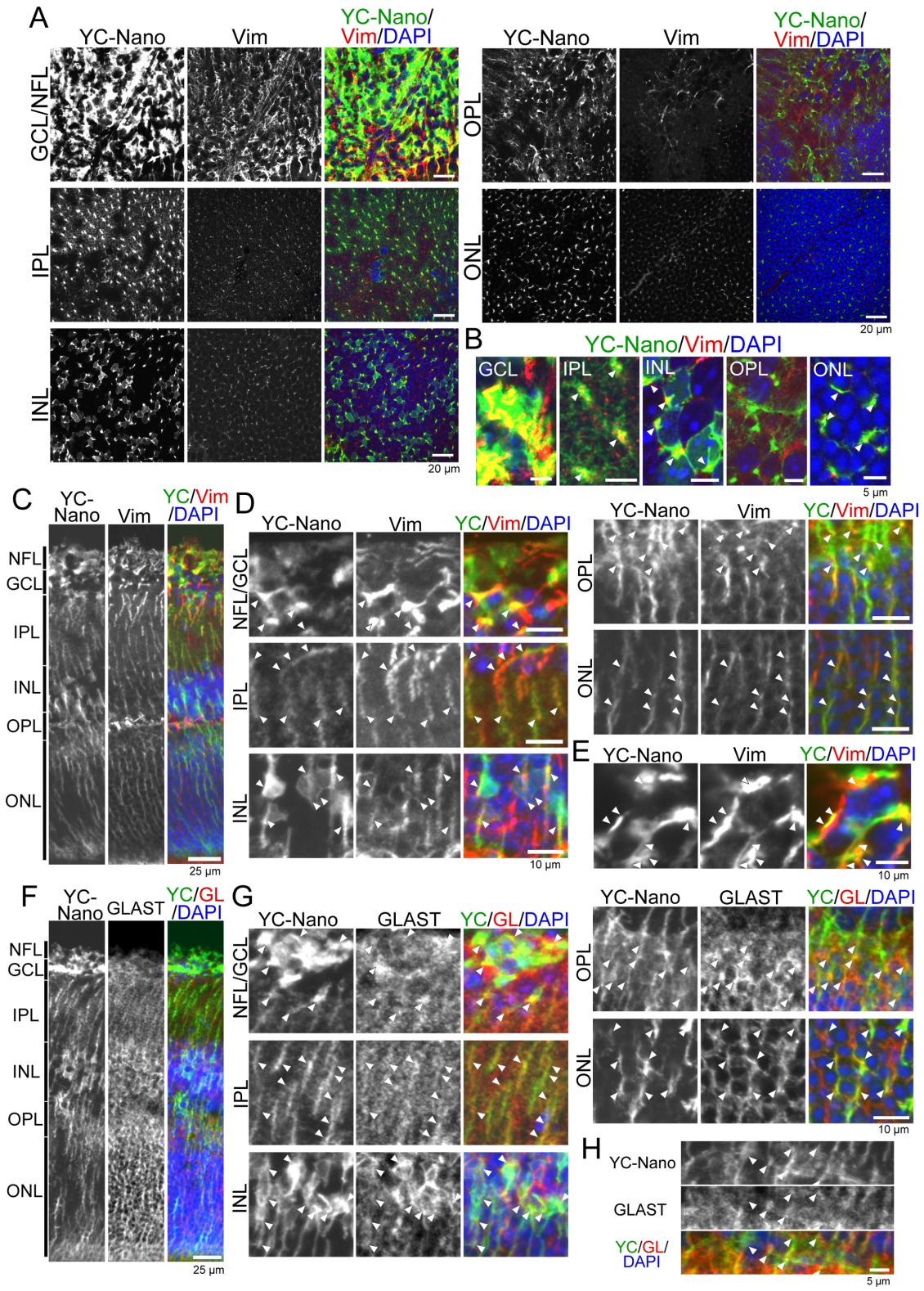

Figure 4. **Müller cells express YC-Nano.** (**A, B**) YC-Nano$^+$ and vimentin$^+$ (Vim) signals in flat-mount retinae showed similar distribution and colocalization in all neural layers, including the GCL, IPL, INL, OPL, and ONL. (**C, D**) The spatial distribution of YC-Nano and Vim in the sliced retinae showed clear colocalization in every layer (*arrows*). (**E**) The tubular structure of the YC-Nano$^+$ signals colocalized with Vim$^+$ signals (*arrows*). (**F, G**) GLAST$^+$ signals also colocalized with YC-Nano$^+$ signals in every layer of the retina. (**H**) The tubular signal was also co-labelled with GLAST$^+$ signals (*arrows*). NFL, nerve fiber layer; GCL, ganglion cell layer; IPL, inner plexiform layer; INL, inner nuclear layer; OPL, outer plexiform layer; ONL, outer nuclear layer.

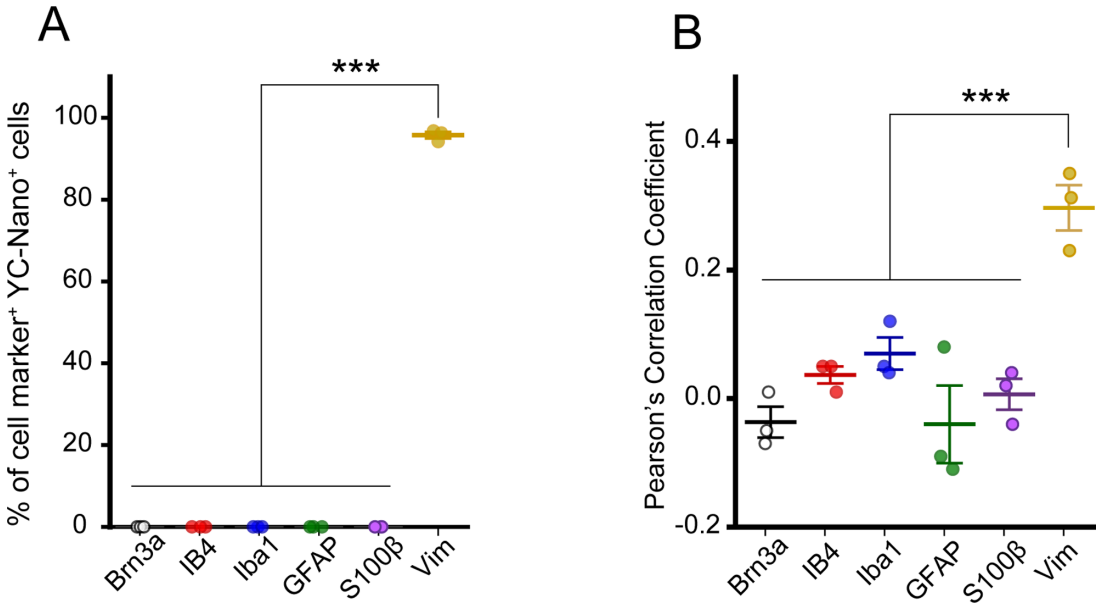

Figure 5. Quantitative analysis of YC-Nano$^+$ cells. (**A**) Counting of YC-Nano$^+$/cell marker$^+$ cells. Brn3a$^+$ (RGC), IB4$^+$ (blood vessels), Iba1$^+$ (microglia), GFAP$^+$, and S100ß$^+$ (astrocytes) signals showed no colocalization with YC-Nano$^+$ signals. Vim$^+$ (Müller cells) signals showed about 95% colocalization with YC-Nano$^+$ signals ($n = 3$ retinae, $^{***}P < 0.0001$, 1-way ANOVA followed by Fisher's LSD test). (**B**) Correlation analysis between GFAP$^+$ and YC-Nano$^+$ signals using Pearson's correlation coefficient (PCC). The PCC value for vimentin was significantly higher (i.e. approximately 0.3) than other cell type markers (i.e. −0.04 to approximately 0.07, $n = 3$ retinae, $^{***}P < 0.0001$, 1-way ANOVA followed by Fisher's LSD test). Data are shown as mean ± SEM.

IPL, many fine process-like structures were observed (see Fig. 1D-a). In the lower part of the IPL and OPL, YC-Nano$^+$ signals showed tubular patterns (see Figs. 1D-b, 1D-d). In the INL, some DAPI signals were incorporated in the YC-Nano$^+$ signals (see Fig. 1D-c). In the outer nuclear layer (ONL), YC-Nano$^+$ signals showed a fiber-like distribution between DAPI-positive regions (see Fig. 1D-e).

We first investigated the colocalization of YC-Nano with the pan-astrocytic marker GFAP in the flat-mount retinae (Fig. 2A). In the NFL, GFAP$^+$ signals formed honeycomb-like patterns that never colocalized with YC-Nano signals (see Fig. 2B, NFL). GFAP$^+$ signals were hardly detected in the other layers (i.e. GCL, IPL, INL, OPL, and ONL). In the retinal slices, GFAP$^+$ signals were detected only in the NFL[38] and did not colocalize with YC-Nano$^+$ signals (see Fig. 2C). Another commonly used astrocytic marker is S100β, which has been shown to colocalize with the astrocytic markers GFAP, SOX9, and SOX2 in the NLF.[39] Here, S100β^+ signals in the NFL showed honeycomb-like patterns and did not colocalize with YC-Nano$^+$ signals (see Fig. 2D).

To test whether retinal ganglion cells express YC-Nano, we investigated the expression patterns of their marker, Brn3a.[40,41] Brn3a$^+$ signals were present in the GCL but did not colocalize with YC-Nano (see Fig. 2A). The endfeet-like YC-Nano$^+$ signals surrounded the Brn3a$^+$ signals. Next, we asked whether YC-Nano$^+$ cells are vascular endothelial cells. Isolectin B4 (IB4) labels endothelial cells as well as some microglia by binding to the rearranged during transfection receptor tyrosine kinase.[42] IB4$^+$ endothelial cells in the GCL and NFL were not labeled with YC-Nano (Fig. 3B). YC-Nano$^+$ process-like signals contacted the blood vessels. IB4$^+$ microglia in the IPL and OPL were not labeled with YC-Nano (see Fig. 3C). We also examined the expression pattern of ionized calcium-binding adapter protein 1 (Iba1), a well-known marker for microglia (see Figs. 3D, 3E). None of the Iba1$^+$ microglia in the flat-mount (in the GCL and IPL) or sliced retinae showed colocalization with YC-Nano$^+$ signals.

We then investigated the expression pattern of the Müller cell marker vimentin. In the GCL and NFL of the flat-mount retina, the majority of vimentin$^+$ process-like structures colocalized with YC-Nano$^+$ signals (Fig. 4). In the IPL through ONL, vimentin$^+$ stalk structures colocalized with relatively strong YC-Nano$^+$ signals (see Figs. 4A, 4B). In the retinal slices, the vimentin$^+$ and YC-Nano$^+$ vertical stalk structures

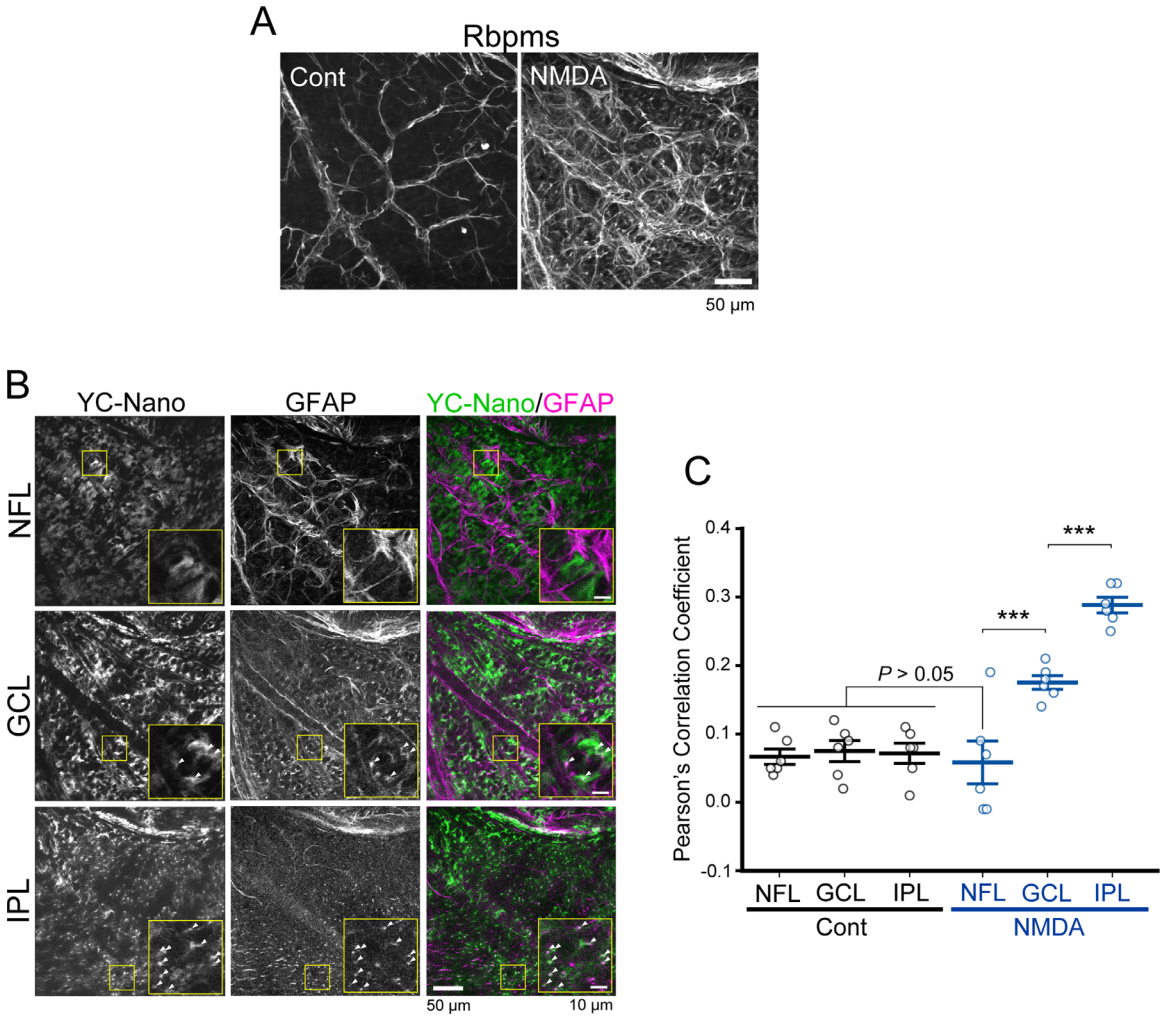

Figure 6. **YC-Nano expression patterns under pathological condition.** (**A**) GFAP$^+$ signals were significantly upregulated at 7 days after intravitreal NMDA injection. The stacked images were obtained from NFL, GCL, and IPL. The NMDA-treated retina showed punctate GFAP$^+$ signals which were hardly detected in the control retina. (**B**) GFAP and YC-Nano expression patterns in each neural layer. In the NFL, GFAP$^+$ signals were observed as fibrous and honeycomb-like pattern and showed no co-localization with YC-Nano$^+$ signals. In the GCL, GFAP$^+$ signals also showed punctate patterns (*arrows*) in addition to fibrous patterns. The punctate GFAP$^+$ signals co-localized with YC-Nano$^+$ signals but the fibrous signals did not. In the IPL, almost all GFAP$^+$ signals were observed as punctate signals (*arrows*). (**C**) Correlation analysis between GFAP$^+$ and YC-Nano$^+$ signals was performed using PCC. The PCC value was not different among the neural layers in control retina and the NMDA-treated NFL. The NMDA-treated GCL and IPL showed higher PPC value than control retina and NMDA-treated NFL ($n = 6$ retinae, $^{***}P < 0.0001$, 1-way ANOVA followed by Fisher's LSD test). Data are shown as mean ± SEM.

(see Fig. 4C) often colocalized (see Fig. 4D). The tubular YC-Nano$^+$ structures also colocalized with vimentin (see Fig. 4E). In the IPL and OPL, the YC-Nano$^+$ signals showed fine process-like structures in addition to stalk structures. We also tested GLAST to examine the expression of YC-Nano in Müller cells (see Fig. 4F). GLAST$^+$ vertical stalk-like structures exhibited fine processes that strongly colocalized with the fine YC-Nano$^+$ signals (see Fig. 4G). The tubular-like YC-Nano$^+$ signals also colocalized with GLAST$^+$ signals (see Fig. 4H). Quantitative analysis revealed that YC-Nano$^+$ signals did not co-localized with RGCs (Brn3a$^+$), blood vessels (IB4$^+$), microglia (Iba1$^+$), astrocytes (GFAP$^+$ or S100β^+) but colocalized with the majority of Müller cells (Vim$^+$; Fig. 5A). To confirm correlation between YC-Nano signals and cell markers, we used Pearson's correlation coefficient (PCC). Similar to the result of cell counting, the PCC value for vimentin was significantly higher (i.e. approximately 0.3) whereas other cell type markers showed near zero (i.e. −0.04 to approximately 0.07; see Fig. 5B).

Because astrocytes have known to become reactive under pathological conditions, such reactive astrocytes may acquire Mlc1 promoter activity. To test this possibility, we investigated the YC-Nano$^+$ signal patterns under excitotoxic condition. At 7 days after intravitreal injection of NMDA, about 70 to 80% of RGCs degenerated (Supplementary Fig. S1A), reproducing the previous result.[37] Retinal astrocytes in the NFL showed an increase in GFAP expression, indicating reactive astrogliosis (Fig. 6A). The GFAP$^+$ reactive astrocytes in the NFL, showing honeycomb-like patterns, did not show any colocalization with YC-Nano$^+$ signals (NFL; see Fig. 6B). The PCC value between GFAP and YC-Nano was similar between control retina and NMDA-treated NFL (see Fig. 6C). These data indicate that retinal astrocytes never show Mlc1 promotor activity even under pathological conditions.

In addition to retinal astrocytes, GFAP$^+$ signals were also observed in Müller cells. The NMDA-treated retina showed many punctate GFAP$^+$ signals, which were hardly detected in the control retina (see Fig. 6A). The newly emerged GFAP$^+$ signals were expressed in the GCL and IPL (see Fig. 6B, Supplementary Fig. S1B) and colocalized with YC-Nano$^+$ signals (see Fig. 6B, Supplementary Fig. S1C), indicating that reactive Müller cells upregulate GFAP expression. S100ß$^+$ and vimentin$^+$ signals in the GCL and IPL were also overlapped with YC-Nano$^+$ signal (see Supplementary Fig. S1D, Supplementary Fig. S1E). Other cell type markers, including Brn3a, Rbpms, IB4, and Iba1 were never colocalized with YC-Nano$^+$ signals (see Supplementary Figs. S1F–S1I). Taken together, our data demonstrate that Mlc1 promoter is active only in Müller cells under both physiological and pathological conditions in the adult retina.

Discussion

Cell type-selective gene manipulation enables us to understand the role of specific cell types in vivo. Our data demonstrates that the Mlc1 promoter can be used for Müller cell-selective gene manipulation in the retina. The *Mlc1* gene encodes the 38 kDa protein that shares sequence homology with K$^+$ channels.[43] The MLC1 protein is localized at the distal part of the astrocytic endfeet and functions together with glial cell adhesion molecule[44]; however, it has never been investigated in the adult retina. We first demonstrated that Mlc1 promoter-mediated gene expression was limited to Müller cells in the adult mouse retina. In agreement with our findings, the single-cell transcriptome database from the human protein atlas showed that the *Mlc1* gene is highly enriched in Müller cells and exhibits minor expression in other cell types, including rod photoreceptors and bipolar cells.[45–47] Our data also demonstrates the regional heterogeneity of YC-Nano$^+$ cells: a relatively high density at the mid-peripheral retina (i.e. 500–1000 µm from the optic nerve head) and a very low density at the peripheral retina. Because the density of Müller cells does not differ between the retinal regions,[30] such differences may be due to cell heterogeneity or different cell activities. Because astrocytes become reactive under pathological condition, YC-Nano expression may be emerged in the reactive astrocytes. However, our data demonstrated that Mlc1 promoter-mediated gene expression is limited in Müller cells even under pathological conditions.

In addition to monitoring cell morphologies, distributions, and densities, the FAST system used in the present study, enables us to either overexpress or knockdown genes. For example, Mlc1-*tTA* mice crossed with tetO mice overexpress the target gene selectively in astrocytes in the brain[34] and Müller cells in the retina. Using Mlc1-*tTS* mice, we can knockdown the gene in Müller cells. Furthermore, in combination with doxycycline treatment, such overexpression or knockdown can be temporally controlled.[31] Müller cells contribute to various ocular diseases, such as age-related macular degeneration,[48] glaucoma,[38,49] and retinal degeneration,[50] and thus Mlc1 promoter-controlled gene manipulation is useful to investigate the pathological roles of Müller cells in various diseases. This technical advantage will enable us to perform successful separation of these two cell types and identification of novel marker for Müller cells in the future study. Overall, our study indicates that the Mlc1 promoter is useful for Müller cell-specific control of gene expression.

Acknowledgments

The authors thank Watanabe, Fukasawa, Tachibana, Koseki, and Aota from the Department of Neuropharmacology, Interdisciplinary Graduate School of Medicine, University of Yamanashi, for technical assistance. We also thank colleagues from the same department for their fruitful discussions. We thank Eva Lasic, PhD, from Edanz (https://jp.edanz.com/ac) for editing a draft of this manuscript.

Grant support: The authors thank members of the Department of Pharmacology, Interdisciplinary Graduate School of Medicine, University of Yamanashi, for their fruitful discussion. This study

was supported by Takeda Science Foundation (Y.S. and S.K.), the Research Foundation for Eye Disease in Aged Individuals (Y.S.), Naito Foundation (S.K.), JSPS KAKENHI Grant Numbers JP18K06481 (Y.S.), JP16K18390 (Y.S.), JP20KK0366 (Y.S.), JP18K14756 (A.N.), JP20K09786 (K.K.), JP17K11478 (K.K.), JP17H06062 (K.T.), JP19H05027 (K.T.), JP20H05896 (K.T.), JP19H04746 (S.K.), JP20H05060 (S.K.), JP20H05902 (S.K.), and JP21H04786 (S.K.), and a Grant-in-Aid for Scientific Research on Innovative Areas, and the technical support platform for promoting research resources "Advanced Bioimaging Support" (JP16H06280; Y.S.). This study was also partially supported by JST Grant CREST number JPMJCR14G2 (S.K.), AMED-CREST (S.K.), and the Frontier Brain Science Grant from the University of Yamanashi (S.K.).

Author contributions: Y.S. designed all the experiments, analyzed all the data, and wrote the manuscript. Y.D. and Y.K. performed the experiments, analyzed the data, and wrote the manuscript. A.N. and K.F.T. provided the transgenic mice and analyzed the data. K.K. and S.K. coordinated the project, analyzed the data, and wrote the manuscript.

Disclosure: **Y. Danjo**, None; **Y. Shinozaki**, None; **A. Natsubori**, None; **Y. Kubota**, None; **K. Kashiwagi**, None; **K.F. Tanaka**, None; **S. Koizumi**, None

* YD and YS contributed equally to this paper.

References

1. Fields RD, Woo DH, Basser PJ. Glial Regulation of the Neuronal Connectome through Local and Long-Distant Communication. *Neuron*. 2015;86:374–386.
2. Zuchero JB, Barres BA. Glia in mammalian development and disease. *Development*. 2015;142:3805–3809.
3. Newman EA. Glial cell regulation of neuronal activity and blood flow in the retina by release of gliotransmitters. *Philos Trans R Soc Lond B Biol Sci*. 2015;370:20140195.
4. Vecino E, Rodriguez FD, Ruzafa N, Pereiro X, Sharma SC. Glia-neuron interactions in the mammalian retina. *Prog Retin Eye Res*. 2016;51:1–40.
5. Allen NJ, Eroglu C. Cell Biology of Astrocyte-Synapse Interactions. *Neuron*. 2017;96:697–708.
6. Chung WS, Allen NJ, Eroglu C. Astrocytes Control Synapse Formation, Function, and Elimination. *Cold Spring Harb Perspect Biol*. 2015;7:a020370.
7. de Pins B, Cifuentes-Diaz C, Farah AT, et al. Conditional BDNF Delivery from Astrocytes Rescues Memory Deficits, Spine Density, and Synaptic Properties in the 5xFAD Mouse Model of Alzheimer Disease. *J Neurosci*. 2019;39:2441–2458.
8. Giralt A, Friedman HC, Caneda-Ferron B, et al. BDNF regulation under GFAP promoter provides engineered astrocytes as a new approach for long-term protection in Huntington's disease. *Gene Ther*. 2010;17:1294–1308.
9. Bei F, Lee HHC, Liu X, et al. Restoration of Visual Function by Enhancing Conduction in Regenerated Axons. *Cell*. 2016;164:219–232.
10. Muller A, Hauk TG, Fischer D. Astrocyte-derived CNTF switches mature RGCs to a regenerative state following inflammatory stimulation. *Brain*. 2007;130:3308–3320.
11. Ballotti R, Nielsen FC, Pringle N, et al. Insulin-like growth factor I in cultured rat astrocytes: expression of the gene, and receptor tyrosine kinase. *The EMBO Journal*. 1987;6:3633–3639.
12. Beck KD, Powell-Braxton L, Widmer HR, Valverde J, Hefti F. Igf1 gene disruption results in reduced brain size, CNS hypomyelination, and loss of hippocampal granule and striatal parvalbumin-containing neurons. *Neuron*. 1995;14:717–730.
13. Duan X, Qiao M, Bei F, Kim IJ, He Z, Sanes JR. Subtype-specific regeneration of retinal ganglion cells following axotomy: effects of osteopontin and mTOR signaling. *Neuron*. 2015;85:1244–1256.
14. Liddelow SA, Barres BA. Reactive Astrocytes: Production, Function, and Therapeutic Potential. *Immunity*. 2017;46:957–967.
15. Luna G, Keeley PW, Reese BE, Linberg KA, Lewis GP, Fisher SK. Astrocyte structural reactivity and plasticity in models of retinal detachment. *Exp Eye Res*. 2016;150:4–21.
16. Danbolt NC. Glutamate uptake. *Progress in Neurobiology*. 2001;65:1–105.
17. Newman E, Reichenbach A. The Muller cell: a functional element of the retina. *Trends in Neurosciences*. 1996;19:307–312.
18. de Melo Reis RA, Cabral-da-Silva M, de Mello FG, Taylor JS. Muller glia factors induce survival and neuritogenesis of peripheral and central neurons. *Brain Research*. 2008;1205:1–11.
19. Garcia M, Forster V, Hicks D, Vecino E. Effects of muller glia on cell survival and neuritogenesis in adult porcine retina in vitro. *Invest Ophthalmol Vis Sci*. 2002;43:3735–3743.

20. Taguchi M, Shinozaki Y, Kashiwagi K, Shigetomi E, Robaye B, Koizumi S. Müller cell-mediated neurite outgrowth of the retinal ganglion cells via P2Y(6) receptor signals. *J Neurochem*. 2016;136:741–751.
21. Kofuji P, Newman EA. Potassium buffering in the central nervous system. *Neuroscience*. 2004;129:1045–1056.
22. Dyer MA, Cepko CL. Control of Muller glial cell proliferation and activation following retinal injury. *Nat Neurosci*. 2000;3:873–880.
23. Goldman D. Müller glial cell reprogramming and retina regeneration. *Nat Rev Neurosci*. 2014;15:431–442.
24. Sarthy PV, Fu M, Huang J. Developmental expression of the glial fibrillary acidic protein (GFAP) gene in the mouse retina. *Cell Mol Neurobiol*. 1991;11:623–637.
25. Drager UC. Coexistence of neurofilaments and vimentin in a neurone of adult mouse retina. *Nature*. 1983;303:169–172.
26. Drager UC, Edwards DL, Barnstable CJ. Antibodies against filamentous components in discrete cell types of the mouse retina. *J Neurosci*. 1984;4:2025–2042.
27. Riepe RE, Norenburg MD. Muller cell localisation of glutamine synthetase in rat retina. *Nature*. 1977;268:654–655.
28. Pow DV, Barnett NL. Changing patterns of spatial buffering of glutamate in developing rat retinae are mediated by the Muller cell glutamate transporter GLAST. *Cell Tissue Res*. 1999;297:57–66.
29. Roesch K, Jadhav AP, Trimarchi JM, et al. The transcriptome of retinal Muller glial cells. *The Journal of Comparative Neurology*. 2008;509:225–238.
30. Wang J, O'Sullivan ML, Mukherjee D, Punal VM, Farsiu S, Kay JN. Anatomy and spatial organization of Muller glia in mouse retina. *The Journal of Comparative Neurology*. 2017;525:1759–1777.
31. Tanaka KF, Ahmari SE, Leonardo ED, et al. Flexible Accelerated STOP Tetracycline Operator-knockin (FAST): a versatile and efficient new gene modulating system. *Biol Psychiatry*. 2010;67:770–773.
32. Tanaka KF, Matsui K, Sasaki T, et al. Expanding the repertoire of optogenetically targeted cells with an enhanced gene expression system. *Cell Rep*. 2012;2:397–406.
33. Kanemaru K, Sekiya H, Xu M, et al. In vivo visualization of subtle, transient, and local activity of astrocytes using an ultrasensitive Ca(2+) indicator. *Cell Rep*. 2014;8:311–318.
34. Shigetomi E, Hirayama YJ, Ikenaka K, Tanaka KF, Koizumi S. Role of Purinergic Receptor P2Y1 in Spatiotemporal Ca(2+) Dynamics in Astrocytes. *J Neurosci*. 2018;38:1383–1395.
35. Shinozaki Y, Shibata K, Yoshida K, et al. Transformation of Astrocytes to a Neuroprotective Phenotype by Microglia via P2Y(1) Receptor Downregulation. *Cell Rep*. 2017;19:1151–1164.
36. Shinozaki Y, Kashiwagi K, Namekata K, et al. Purinergic dysregulation causes hypertensive glaucoma-like optic neuropathy. *JCI Insight*. 2017;2:e93456.
37. Takeda A, Shinozaki Y, Kashiwagi K, et al. Microglia mediate non-cell-autonomous cell death of retinal ganglion cells. *Glia*. 2018;66:2366–2384.
38. Shinozaki Y, Koizumi S. Potential roles of astrocytes and Muller cells in the pathogenesis of glaucoma. *J Pharmacol Sci*. 2021;145:262–267.
39. Fischer AJ, Zelinka C, Scott MA. Heterogeneity of glia in the retina and optic nerve of birds and mammals. *PLoS One*. 2010;5:e10774.
40. Badea TC, Cahill H, Ecker J, Hattar S, Nathans J. Distinct roles of transcription factors brn3a and brn3b in controlling the development, morphology, and function of retinal ganglion cells. *Neuron*. 2009;61:852–864.
41. Nadal-Nicolás FM, Jiménez-López M, Sobrado-Calvo P, et al. Brn3a as a marker of retinal ganglion cells: qualitative and quantitative time course studies in naive and optic nerve-injured retinas. *Invest Ophthalmol Vis Sci*. 2009;50:3860–3868.
42. Boscia F, Esposito CL, Casamassa A, de Franciscis V, Annunziato L, Cerchia L. The isolectin IB4 binds RET receptor tyrosine kinase in microglia. *J Neurochem*. 2013;126:428–436.
43. Boor PK, de Groot K, Waisfisz Q, et al. MLC1: a novel protein in distal astroglial processes. *J Neuropathol Exp Neurol*. 2005;64:412–419.
44. Brignone MS, Lanciotti A, Camerini S, et al. MLC1 protein: a likely link between leukodystrophies and brain channelopathies. *Front Cell Neurosci*. 2015;9:66.
45. Thul PJ, Akesson L, Wiking M, et al. A subcellular map of the human proteome. *Science*. 2017;356:eaal3321.
46. Uhlen M, Fagerberg L, Hallstrom BM, et al. Proteomics. Tissue-based map of the human proteome. *Science*. 2015;347:1260419.
47. Uhlen M, Zhang C, Lee S, et al. A pathology atlas of the human cancer transcriptome. *Science*. 2017;357:eaan2507.
48. Menon M, Mohammadi S, Davila-Velderrain J, et al. Single-cell transcriptomic atlas of the human retina identifies cell types associated with

age-related macular degeneration. *Nat Commun*. 2019;10:4902.

49. Harada T, Harada C, Nakamura K, et al. The potential role of glutamate transporters in the pathogenesis of normal tension glaucoma. *J Clin Invest*. 2007;117:1763–1770.
50. Voigt AP, Binkley E, Flamme-Wiese MJ, et al. Single-Cell RNA Sequencing in Human Retinal Degeneration Reveals Distinct Glial Cell Populations. *Cells*. 2020;9:438.